The unsteady drag force on a cylinder immersed in a dilute granular flow

Rahul Bharadwaj and Carl Wassgren
School of Mechanical Engineering, Purdue University, West Lafayette, Indiana 47907-2088

Roberto Zenit
Instituto de Investigaciones en Materiales, Universidad Nacional Autónoma de México, Apartado Postal 70-360, Ciudad Universitaria, Coyoacán Distrito Federale 04510, Mexico

(Received 30 November 2005; accepted 3 March 2006; published online 19 April 2006)

This paper presents results from hard-particle discrete element simulations of a two-dimensional dilute stream of particles accelerating past an immersed fixed cylinder. Simulation measurements of the drag force F_d are expressed in terms of a dimensionless drag coefficient, $C_d = F_d / \left[\frac{1}{2}\rho\nu U^2 (D+d)\right]$, where ρ is the particle density, ν is the upstream solid fraction, U is the upstream instantaneous velocity, and D and d are the cylinder and particle diameters, respectively. Measurements indicate that the cylinder's unsteady drag coefficient does not vary significantly from its steady (nonaccelerating) drag coefficient for both frictionless and frictional particles implying that the added mass for the flow is negligible. However, the drag coefficient is larger than its nominal value during an initial transient stage, during which a shock wave develops in front of the cylinder. Once the shock has developed, the drag coefficient remains constant despite the stream's acceleration. The duration of the shock development transient stage is a function of the number of particle/cylinder collisions. © *2006 American Institute of Physics*. [DOI: 10.1063/1.2191907]

I. INTRODUCTION

A granular material consists of an assembly of solid particles dispersed in a surrounding fluid or vacuum. In a granular flow, the momentum transport due to particle motion and particle-particle interactions is a significant component of the overall momentum transport. Granular flows are common in a number of industries, including those that manufacture or process chemicals, pharmaceuticals, powdered ceramics, food stuffs, ores, and building materials. Granular flows are also observed in many natural processes such as avalanches, landslides, dune formation, and planetary ring formation.

Wassgren *et al.*[1] and Chehata *et al.*[2] present a summary of some of the previous studies concerning steady granular flows past obstacles for both dilute and dense flows. In particular, Wassgren *et al.*[1] found that the drag coefficient for a cylinder, with diameter D held stationary in a constant-speed, two-dimensional, *dilute* (also commonly referred to as a granular gas) jet of monodisperse particles, with diameter d and density ρ, depends on the flow Knudsen number, $\mathrm{Kn} = \pi / [8\nu(D/d)]$, where ν is the jet's upstream solid fraction, with a secondary dependence on the upstream Mach number in the subsonic range, where the Mach number is defined as $\mathrm{Ma} = U/c$, where U is the upstream jet speed and c is the upstream speed of sound in the jet. The drag coefficient is defined as $C_d = F_d / \left[\frac{1}{2}\rho\nu U^2 (D+d)\right]$, where F_d is the drag force acting on the cylinder. These dilute granular flows also exhibit compressible flow phenomena such as bow shocks and expansion fans; however, unlike traditional gas flows, these phenomena show little dependence on the flow's Mach number.[1] Indeed, measurements of the cylinder's bow shock angle indicate that it is independent of the Mach number, a trend quite different from typical gas dynamics flows.

Previous studies have focused on steady granular flows; however, many granular flows with obstacles are, in fact, not steady. For example, the impact of an object into a dense granular bed, with applications including soil impact penetrometers, military ballistics, and planetary crater dynamics (see, for example, Boguslavskii *et al.*,[3] Forrestal and Luk,[4] and, more recently, Ciamarra *et al.*[5] and Uehera *et al.*[6]), is an inherently unsteady flow. Unsteady flow around immersed objects is also observed in the segregation of impurities due to forced vibrations.[7] Yet another example is the transient stage of an avalanche or rock slide around an obstacle such as a bridge pylon or other man-made structures.[8]

Despite their significance, the forces on obstacles in unsteady granular flows have not been extensively studied. It is well known that for fluid flows, even those that are inviscid, the unsteady drag force acting on an object is larger than the steady drag force due to an "added mass" effect.[9] The relative significance of the added mass increases as the ratio of the fluid density to the object density increases. Similar added mass investigations have not been performed for granular flows despite the fact that in many cases the surrounding flow bulk density is of the same order of magnitude as the object density. This paper presents results from computational studies investigating the added mass for an accelerating dilute granular jet flowing around an immersed cylinder.

II. COMPUTATIONAL MODEL

An event-driven, hard-particle discrete-element simulation method is utilized in this study. The event-driven, hard-particle method is efficient for modeling dilute granular flows where the time between particle collisions is large. Furthermore, the hard-particle assumption necessitates that

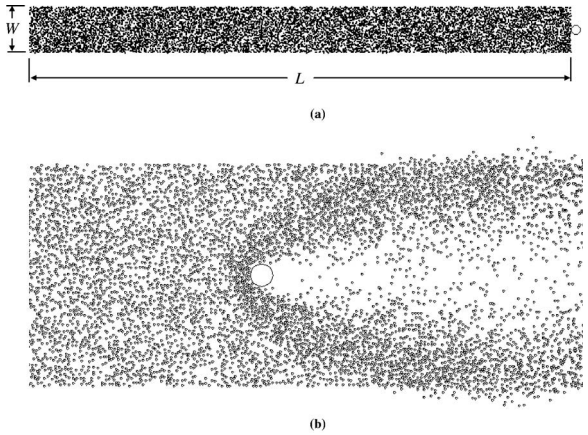

FIG. 1. (a) Snapshot from a simulation showing the particles placed upstream of the fixed cylinder with baseline parameters given in Table I. The flow is from left to right and the cylinder is fixed at the far right. (b) Snapshot taken at a later time showing the formation of a bow shock upstream of the cylinder. Note that the snapshot zooms in on the cylinder for clarity.

only binary, nearly instantaneous collisions predominate in the flow. Campbell and Brennen[10] describe the hard-particle method in detail.

The algorithm is implemented here in two dimensions. The workspace consists of a fixed cylinder of diameter D immersed in a jet of circular particles (infinitely long cylinders) of uniform diameter d and density ρ. The jet has a spanwise width W, which is symmetric about the cylinder, and has a streamwise length L. The cylinder is initially positioned just downstream of the jet (refer to Fig. 1). Particles are randomly placed in the jet, taking care to avoid overlap with other particles, and have zero initial velocity but a constant horizontal acceleration. Both free jet and periodic boundaries were used in the simulations and gravity is neglected. No differences were observed between the two types of boundary conditions when the jet width was sufficiently large (to be discussed in the following section). Note that a fixed cylinder in an accelerating jet, and a fixed jet and an accelerating cylinder are equivalent systems.

In most of the simulations the upstream granular temperature is zero since in a dissipative granular system (one with inelastic collisions and/or friction) the granular temperature approaches zero unless the particles are subjected to an energy source. Hence, a zero granular temperature assumption for the incoming particle stream is reasonable. However, in order to investigate the effects of a finite Mach number upstream flow, several of the simulations included nonzero upstream granular temperature and periodic boundary conditions (to maintain a constant solid fraction). Random streamwise and spanwise velocity fluctuations were added to the granular stream ten cylinder diameters upstream of the cylinder. The fluctuations were added at the given location in order to minimize the dissipation of the granular temperature as the jet approached the cylinder, yet be sufficiently far upstream of the cylinder to avoid interactions with the cylinder's bow shock wave. The magnitude of the fluctuations was sufficiently small relative to the free stream in order to maintain a supersonic, but finite Mach number flow. Subsonic flows were avoided since in a subsonic flow the entire flow field is affected by the presence of the cylinder and the upstream boundary conditions can affect the measured drag force.

The collision time between two particles is straightforward to calculate. A particle i moves in a ballistic trajectory between collisions:

$$\mathbf{x}_i = \tfrac{1}{2}\ddot{\mathbf{x}}_{0i}(t - t_{0i})^2 + \dot{\mathbf{x}}_{0i}(t - t_{0i}) + \mathbf{x}_{0i}, \tag{1}$$

where $\mathbf{x}_i$ is the position of the particle at time t, $\ddot{\mathbf{x}}_{0i}$ is the particle's acceleration, t_{0i} is the time of the last collision involving this particle, and $\dot{\mathbf{x}}_{0i}$ and $\mathbf{x}_{0i}$ are the particle's velocity and position, respectively, immediately following the last collision. Two particles will collide when they are separated by a distance equal to the sum of their radii:

$$|\mathbf{x}_i - \mathbf{x}_j| = \tfrac{1}{2}(d_i + d_j). \tag{2}$$

Substituting Eq. (1) into Eq. (2) and simplifying gives the time of a collision as the solution to the fourth-order polynomial:

$$a_4 t^4 + a_3 t^3 + a_2 t^2 + a_1 t + a_0 = 0, \tag{3}$$

where

$$\begin{aligned} a_4 &= A_x^2 + A_y^2 + A_z^2, \\ a_3 &= 2(A_x B_x + A_y B_y + A_z B_z), \\ a_2 &= 2(A_x C_x + A_y C_y + A_z C_z) + B_x^2 + B_y^2 + B_z^2, \\ a_1 &= 2(B_x C_x + B_y C_y + B_z C_z), \\ a_0 &= C_x^2 + C_y^2 + C_z^2 - \tfrac{1}{4}(d_i + d_j)^2, \end{aligned} \tag{4}$$

and

$$\begin{aligned} \mathbf{A} &= \tfrac{1}{2}(\ddot{\mathbf{x}}_{0i} - \ddot{\mathbf{x}}_{0j}), \\ \mathbf{B} &= -\ddot{\mathbf{x}}_{0i} + \dot{\mathbf{x}}_{0i} + \ddot{\mathbf{x}}_{0j} - \dot{\mathbf{x}}_{0j}, \\ \mathbf{C} &= \tfrac{1}{2}\ddot{\mathbf{x}}_{0i} t_{0i}^2 - \dot{\mathbf{x}}_{0i} + \mathbf{x}_{0i} - \tfrac{1}{2}\ddot{\mathbf{x}}_{0j} t_{0j}^2 + \dot{\mathbf{x}}_{0j} - \mathbf{x}_{0j}. \end{aligned} \tag{5}$$

Equation (3) reduces to a quadratic polynomial for a two-particle collision since $\ddot{\mathbf{x}}_{0i} = \ddot{\mathbf{x}}_{0j}$. However, for a particle/cylinder collision, the fourth-order polynomial must be solved since the particle has nonzero acceleration, in general, and the cylinder has zero acceleration. The polynomial in Eq. (3) is factored into two quadratic equations using Bairstow's method[11] that are then solved using the quadratic formula. Only real collision times that are greater than the current time are considered. The smallest real collision time that is greater than the current time is added to the list of possible future collisions. In order to reduce the number of particle/particle contact checks, a neighboring cell contact detection algorithm[12] is also implemented.

Particle states immediately following a collision are determined using a hard-particle dynamics model. Three parameters are included in the model, including a normal coefficient of restitution ε_N, a stick-slip tangential coefficient of restitution ε_{S0}, and a coefficient of sliding friction μ. Details

on how the post-collision particle states are related to the three parameters and the pre-collision states are given in Wassgren *et al.*[1]

The average force **F** acting on the cylinder over time T is related to the momentum impulse **J** acting on the cylinder, by

$$\mathbf{F} = \frac{1}{T}\sum_{t}^{t+T} \mathbf{J}. \tag{6}$$

Since the granular jet is accelerating, a fixed value of T would result in poor time resolution when the jet velocity is large. Hence, T is chosen instead to be the time it takes a fixed number of particle/cylinder impacts to occur (50 impacts for the cases considered here). At small jet speeds, T is typically large, while at large jet speeds, T is typically small. Even after averaging the drag force over tens of impacts, large fluctuations are still observed in the drag force measurements. Therefore, 50 simulations using random initial particle positions are run for each set of unsteady drag force conditions and their results are ensemble averaged. An ensemble average of the "instantaneous" time required to obtain N particle/cylinder collisions is determined as:

$$\langle T \rangle_N = \frac{1}{N}\sum_{1}^{N} T. \tag{7}$$

In many of the simulations, a bow shock structure[1] is observed [see Fig. 1(b)]. In order to characterize the size of this shock, a shock thickness δ is defined as the distance from the cylinder's leading edge along the centerline to the first point in the flow where the particle stream has a speed equal to the jet free stream speed. The centerline speed is averaged in a $4d \times 4d$ square region symmetric about the centerline in order to minimize fluctuations. The shock thickness measurements were also ensemble averaged over the 50 simulations similar to what has been described previously. Note that at the smallest solid fractions ($\leqslant 0.1$), the shock structure is not well defined, and hence a shock thickness measurement is meaningless.

III. RESULTS AND DISCUSSION

A summary of the investigated simulation parameters is given in Table I. First, the steady drag force acting on the cylinder was measured for nonaccelerating flows. Previous work by Wassgren *et al.*[1] found, using both hard- and soft-particle discrete-element simulations, that the drag force, expressed in terms of a drag coefficient C_d,

$$C_d = \frac{F_d}{\frac{1}{2}\rho\nu U^2 (D+d)}, \tag{8}$$

is a function of the flow Knudsen number Kn,

$$\mathrm{Kn} = \frac{\pi d}{8\nu D}, \tag{9}$$

where F_d is the drag force acting on the cylinder, ρ is the jet particle mass density, ν is the free stream solid fraction, U is the free stream speed, D is the cylinder diameter, and d is the jet particle diameter. The drag coefficient is independent of Mach number for supersonic conditions but does show a strong dependence for subsonic Mach numbers. Most of the current simulations are performed with zero upstream granular temperature, and hence the upstream Mach number is infinite. These results will be reported first. A typical initial flow configuration is shown in Fig. 1(a).

TABLE I. Baseline parameters used in the simulations.

Particle diameter d (mm)	1
Particle density ρ (kg/m^3)	1000
Cylinder diameter D (mm)	10
Normal coefficient of restitution ε_N	0.95
Friction coefficient μ	0
Stick-slip tangential coefficient of restitution ε_{S0}	−1
Jet width W (mm)	100
Jet length L (mm)	1000
Upstream acceleration $\ddot{\mathbf{x}}_{0i}$ (m/s^2)	0.1
Upstream initial velocity U (m/s)	0
Upstream solid fraction ν	0.2
Upstream granular temperature T (mm^2/s^2)	0
Upstream Knudsen number Kn	0.2
Upstream Mach number Ma	∞

Figure 2 plots the "instantaneous," ensemble-averaged drag force as a function of the instantaneous upstream jet velocity for several jet accelerations (the initial jet velocity was zero in all of the simulations). It is evident that the drag force scales as the square of the upstream velocity, a scaling identical to that for corresponding steady flows.[1] Figure 3 demonstrates that the particle/cylinder collision rate is proportional to the instantaneous jet velocity regardless of jet acceleration, again a result identical to that for steady flows.[1]

The drag data do, however, exhibit an initial transient region. This transient is more easily observed in Fig. 4, where the drag coefficient is plotted as a function of time for

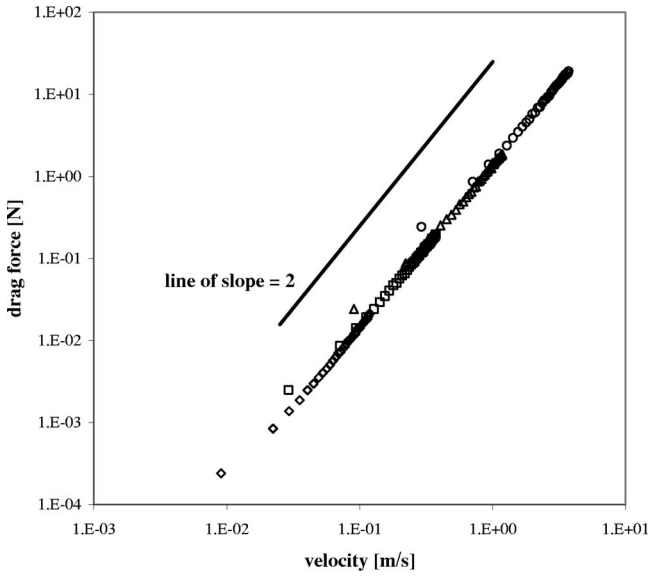

FIG. 2. The instantaneous drag force plotted as a function of instantaneous upstream velocity for accelerations of 0.01 (◇), 0.1 (□), 1 (△), and 10 (○) m/s^2, with the remaining conditions given in Table I.

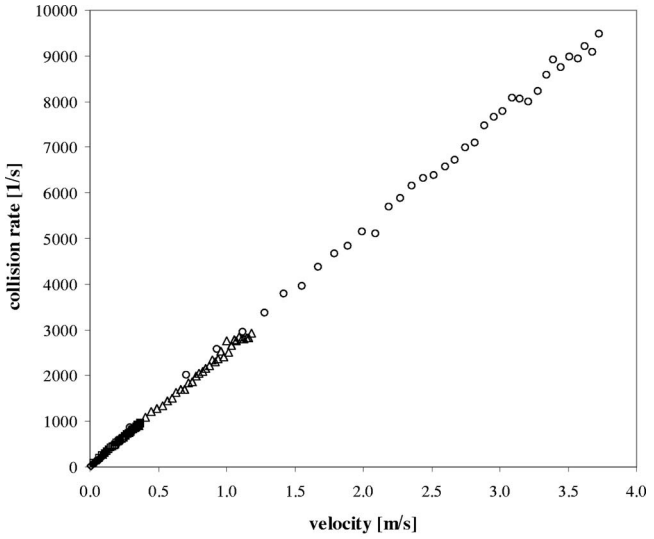

FIG. 3. The particle/cylinder collision rate plotted as a function of instantaneous upstream velocity for accelerations of 0.01 (◇), 0.1 (□), 1 (△), and 10 (○) m/s^2, with the remaining conditions given in Table I.

several jet accelerations. There is clearly an initial period in which the drag coefficient is larger than the corresponding steady drag coefficient with the drag coefficient monotonically decreasing to the steady drag coefficient value as the jet continues to accelerate. The time required for the transient to disappear decreases with increasing jet acceleration. Plotting the same drag coefficient data as a function of the cumulative number of particle/cylinder collisions (Fig. 5) collapses the data for all of the jet accelerations with the initial transient becoming negligible after approximately 600 particle/cylinder collisions. The cause for this initial transient will be discussed later, but it is important to mention at this point that it is not a direct function of the jet acceleration.

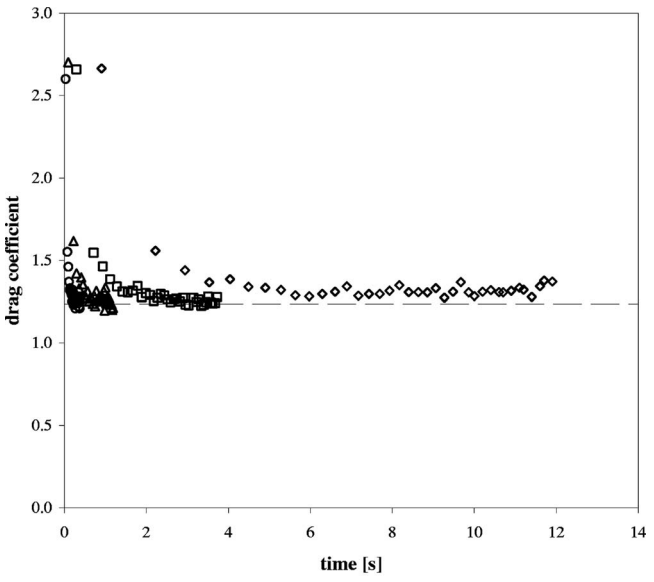

FIG. 4. The unsteady drag coefficient plotted as a function of the simulation time for accelerations of 0.01 (◇), 0.1 (□), 1 (△), and 10 (○) m/s^2, with the remaining conditions given in Table I. The steady drag coefficient value (particles with zero acceleration) is shown as a dashed line.

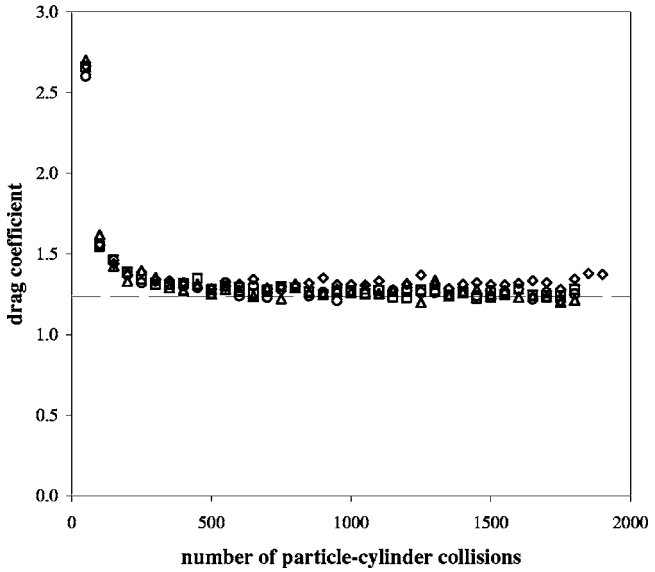

FIG. 5. The unsteady drag coefficient plotted as a function of the number of particle/cylinder collisions for accelerations of 0.01 (◇), 0.1 (□), 1 (△), and 10 (○) m/s^2, with the remaining conditions given in Table I. The steady drag coefficient value (particles with zero acceleration) is shown as a dashed line.

The average unsteady drag coefficient C_{du} is obtained by eliminating the initial transients that are observed in Fig. 5. A steady drag coefficient, C_{ds} was determined by taking the average of three steady flow simulations (zero acceleration) with upstream velocities of 0.1, 0.5, and 1.0 m/s and the conditions given in Table I. The drag coefficient ratio C_{du}/C_{ds} is shown as a function of acceleration for various solid fractions ν in Fig. 6. It is evident that the unsteady drag coefficient does not vary significantly from the steady (zero acceleration) drag coefficient despite a three order of magni-

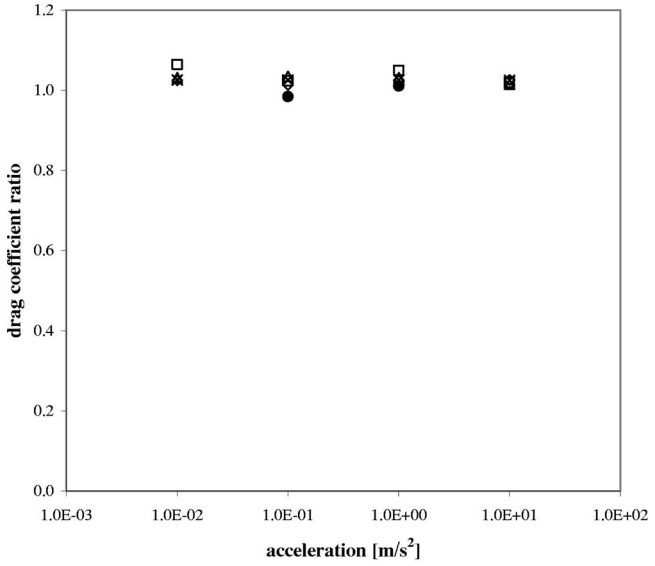

FIG. 6. The ratio of unsteady-to-steady drag coefficient plotted as a function of upstream particle acceleration for solid fractions of 0.1 (△), 0.2 (□), 0.3 (×), and 0.4 (◇), with the remaining conditions given in Table I. The closed symbols (●) indicate flows with upstream Mach numbers ranging between 1 and 2, with the remaining conditions given in Table I.

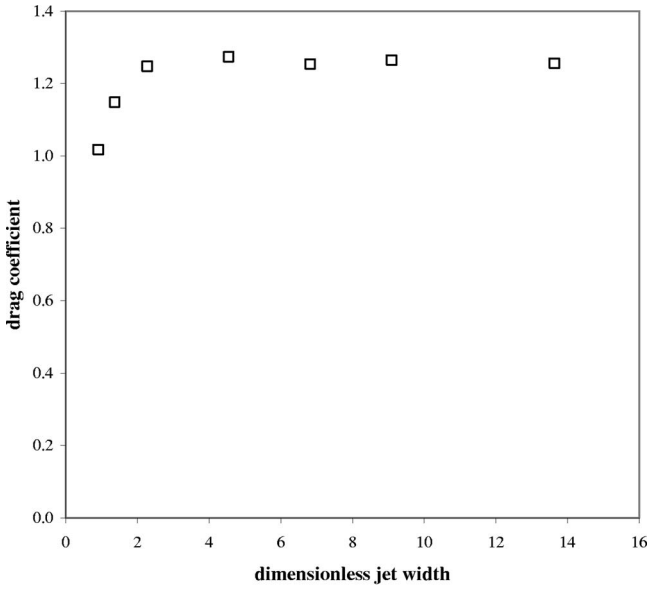

FIG. 7. The unsteady drag coefficient plotted against the jet width W normalized by the effective cylinder diameter $D+d$.

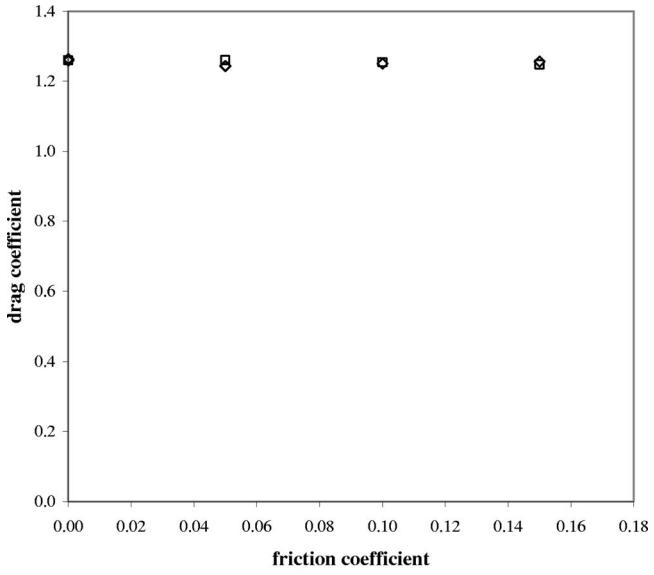

FIG. 8. The drag coefficient plotted against the friction coefficient for stick-slip tangential coefficient values of $\varepsilon_{S0}=0.35$ ($\diamond$) and 1.0 ($\square$), with the remaining conditions given in Table I.

tude variation in jet acceleration. Hence, there appears to be no discernable added mass for the given conditions. Note that for a perfect fluid the ratio of the added mass force F_U to the steady drag force F_S is

$$\frac{F_U}{F_S}=\frac{\rho_F(\pi/4)D^2a}{C_{\mathrm{ds}}\frac{1}{2}\rho_F U^2 D}=\frac{\pi Da}{2C_{\mathrm{ds}}U^2}, \tag{10}$$

where ρ_F is the fluid density and C_{ds} is the steady drag coefficient (of order one). For the conditions investigated here $D\sim 10^{-2}$ m, $a\sim 1$ m/s^2, and $U\sim 10^{-1}$ m/s, and thus for a perfect fluid, the unsteady drag force has approximately the same magnitude as the steady drag force.

Several simulations were performed using the baseline simulation parameters (Table I) in order to determine what influence the workspace dimensions, i.e., jet streamwise length L and spanwise width W, have on the drag coefficient. In Fig. 7, where the drag coefficient is plotted as a function of the jet width (normalized by $D+d$) for the baseline parameters, the drag coefficient is observed to increase with increasing jet width for $W/(D+d)$ less than approximately 2.5. A corresponding reduction in the particle/cylinder collision rate is observed for these conditions indicating that the drag coefficient reduction occurs due to fewer particle/cylinder impacts. For larger dimensionless jet widths, the drag coefficient is independent of the jet width. Based on the previous discussion concerning the time required to reach a constant drag coefficient, the jet streamwise length needs only to be long enough to result in a sufficient number of particle/cylinder impacts to get past the initial transient stage (approximately 600 impacts for the baseline parameters).

The dependence of the unsteady drag coefficient on the particle/particle and particle/cylinder tangential collision properties (friction coefficient μ, and stick-slip coefficient of restitution ε_{S0}) was also investigated. In order to simplify the investigation, the particle/particle and particle/cylinder tangential properties were set equal (i.e., $\mu_{\mathrm{PP}}=\mu_{\mathrm{PC}}$ and $\varepsilon_{S0,\mathrm{PP}}=\varepsilon_{S0,\mathrm{PC}}$). The friction coefficients for the simulations ranged from zero to 1.0 for two values of the stick-slip tangential coefficient of restitution: $\varepsilon_{S0}=0.35$ and $\varepsilon_{S0}=1.0$. The phenomenon of inelastic collapse was observed for friction coefficients greater than 0.15 for both the values of ε_{S0}. This appears to be the results of the formation of force chains in the flow. As shown in Fig. 8, the unsteady drag coefficient shows no significant variation with either acceleration or tangential coefficient of restitution ε_{S0}, for friction coefficients up to 0.15.

Simulations with finite, supersonic Mach numbers were also investigated. Figure 9 plots the upstream Mach number as a function of the distance from the cylinder's leading edge for one of the investigated flows (refer to Wassgren *et al.*[1] for

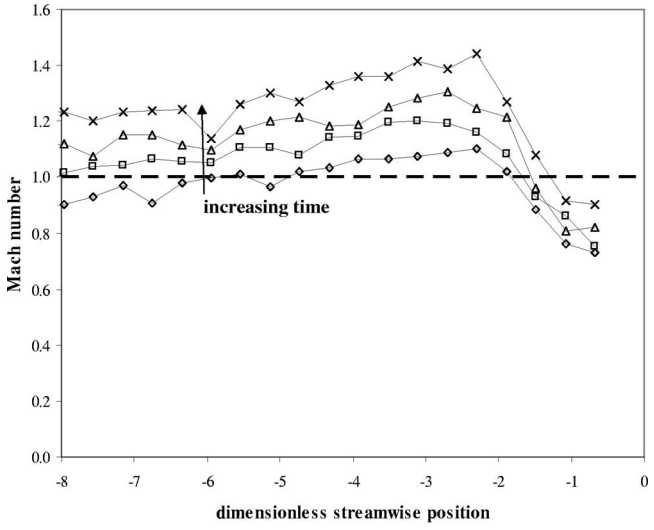

FIG. 9. The flow Mach number plotted as a function of the position upstream of the cylinder's center for a flow with nonzero granular temperature and the remainder of the conditions given in Table I. The streamwise distance is made dimensionless by the cylinder diameter D.

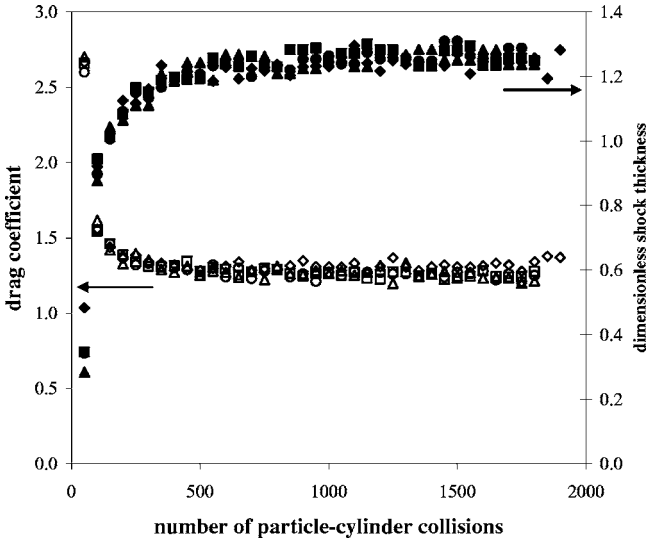

FIG. 10. The unsteady drag coefficient (open symbols) and shock thickness (closed symbols) for accelerations of 0.01 (♦), 0.1 (■), 1 (▲), and 10 (●) m/s^2 plotted against the number of particle/cylinder collisions, with the remaining conditions given in Table I.

a discussion on how the Mach number is determined) with the remaining conditions given in Table I. The Mach number increases as the particles move downstream of the location at which the velocity fluctuations were added to the flow (ten cylinder diameters upstream of the cylinder center) reflecting the fact that granular flows tend toward infinite Mach number without an external energy source. Since the flow does not have a well defined Mach number, the largest Mach number, which occurs just upstream of the bow shock wave, is used as a reference. Figure 6 includes data for the ratio of the unsteady to steady drag coefficient as a function of stream acceleration for Mach numbers ranging between 1 and 2 with the remaining conditions given in Table I. The steady drag coefficients were determined for identical Mach number conditions as the unsteady flows. As with the infinite Mach number cases, the supersonic Mach number cases indicate that for the conditions investigated, there is no discernible added mass.

In order to explain the initial transient observed in the drag coefficient data (Fig. 5), the thickness δ of the bow shock wave that forms on the leading edge of the cylinder is plotted [in normalized form as $\delta/(D+d)$] as a function of the number of cumulative particle/cylinder collisions in Fig. 10 along with the drag coefficient for various jet accelerations. The bow shock thickness is defined as the distance along the flow centerline from the cylinder leading edge to the first point in the flow where the local speed is equal to the jet's free stream speed. Two interesting points can be observed from the data. First, similar to the drag coefficient, the shock goes through an initial transient stage where the shock thickness increases and asymptotes to a constant value despite the fact that the jet continues to accelerate. Hence, it appears that the initial transient in the drag coefficient is, in fact, due to the development of the bow shock wave and not a result of the jet acceleration. Second, the shock thickness is not only independent of the instantaneous velocity, but it is also independent of the jet acceleration. This observed insensitivity of the shock characteristics to the flow speed is similar to what was reported in a previous study.[1,14]

IV. CONCLUSIONS

The unsteady drag coefficients for the constant acceleration dilute granular flows investigated here have the same values as the corresponding steady flow (zero acceleration) drag coefficients. Hence, the added mass for these flows is negligible. This result is significantly different than what occurs in ordinary incompressible fluid flows. In an incompressible fluid, an accelerating object must also accelerate the surrounding fluid (with an equivalent "added mass") and, hence, the accelerating drag force is greater than the nonaccelerating drag force. However, if the speed of sound in the fluid is small compared to the flow velocity, then the added mass will also depend on the Mach number since the region of fluid that is affected by the acceleration will depend on the Mach number. For a dilute granular flow, the Mach numbers are typically in the supersonic range[13] (indeed, for many of the cases investigated here the Mach numbers are infinite). Since the bow shock characteristics are independent of the effective Mach number,[14] the region of granular material affected by the acceleration does not significantly change and hence the added mass is unaffected by the acceleration. Knowing that a dilute granular flow's added mass is negligible is particularly useful since it greatly simplifies the determination of forces in unsteady, dilute granular flows.

Drag coefficients larger than the steady drag coefficients were observed during the initial, transient stages of the flow due to the formation of a bow shock wave in front of the cylinder. This phenomenon can also be considered an unsteady effect, but it is not specifically linked to the accelerating jets investigated here since the same shock formation transient occurs even for jets with constant velocity. Once the shock structure forms, it appears to be insensitive to the flow velocity and acceleration. Dilute granular flows with time constants shorter than or with roughly the same magnitude as the shock formation time constant (which, based on the work presented here, is related to the cumulative number of particle/cylinder collisions) should factor in this unsteady drag effect. Examples of such flows include high-frequency oscillating objects/flows, or short-duration impact events.

It should be reiterated that the results presented here are specifically for dilute-supersonic granular flows. It is not clear from this work how significant added mass effects will be in dense granular flows or dilute, subsonic flows since in both of these flow cases the region of flow that is affected by the presence of the accelerating object is much larger than in the dilute-supersonic case. The dense flow case is of particular interest since most terrestrial granular flows, such as granular impacts, occur in this regime.

ACKNOWLEDGMENTS

We gratefully acknowledge the support of the National Aeronautics and Space Administration agency through the *Fluid Physics: Research and Flight Experiment Opportunities* program (NRA 01-OBPR-02). One of the authors (R.Z.)

acknowledges the support of UNAM-PAPIIT Grant No. 102303.

[1] C. R. Wassgren, J. A. Cordova, R. Zenit, and A. Karion, "Dilute granular flow around an immersed cylinder," Phys. Fluids **15**, 3318 (2003).
[2] D. Chehata, R. Zenit, and C. R. Wassgren, "Dense granular flow around an immersed cylinder," Phys. Fluids **15**, 1622 (2003).
[3] Y. Boguslavskii, S. Drabkin, and A. Salman, "Analysis of vertical projectile penetration in granular soils," J. Phys. D **29**, 905 (1996).
[4] M. J. Forrestal and V. K. Luk, "Penetration into soil targets," Int. J. Impact Eng. **12**, 427 (1992).
[5] M. P. Ciamarra, A. H. Lara, A. T. Lee, D. I. Goldman, I. Vishik, and H. L. Swinney, "Dynamics of drag and force distributions for projectile impact in a granular medium," Phys. Rev. Lett. **92**, 194301 (2004).
[6] J. S. Uehera, M. A. Ambrose, R. P. Ojha, and D. J. Durian, "Low-speed impact craters in loose granular media," Phys. Rev. Lett. **90**, 194301 (2003).
[7] K. Liffman, K. Muniandy, M. Rhodes, D. Gutteridge, and G. Metcalfe, "A segregation mechanism in a vertically shaken bed," Granular Matter **3**, 205 (2001).
[8] Y. C. Tai, J. M. N. T. Gray, K. Hutter, and S. Noelle, "Flow of dense avalanches past obstructions," Ann. Glaciol. **32**, 281 (2001).
[9] C. S. Yih, *Fluid Dynamics* (West River, Ann Arbor, MI, 1969).
[10] C. S. Campbell and C. E. Brennen, "Computer simulation of granular shear flows," J. Fluid Mech. **151**, 167 (1985).
[11] J. D. Hoffman, *Numerical Methods for Engineers and Scientists* (Marcel Dekker, New York, 2001).
[12] M. E. Lasinski, J. S. Curtis, and J. F. Pekny, "Effect of system size on particle-phase stress and microstructure formation," Phys. Fluids **16**, 265 (2004).
[13] E. C. Rericha, C. Bizon, and H. L. Swinney, "Shocks in supersonic sand," Phys. Rev. Lett. **88**, 014302 (2002).
[14] There are apparent discrepancies between two recently published papers concerning shock wave characteristics in granular flows. Wassgren *et al.* (Ref. 1) report that granular shock wave characteristics are insensitive to the upstream Mach number while Heil *et al.* (Ref. 15) report that the shock angle follows a Mach wave relation. The work by Wassgren *et al.* investigates compressible granular flows (shock waves), while Heil *et al.* investigate shallow free surface flows (hydraulic jumps rather than shock waves). Although there are similarities between free surface and compressible flows, care should be taken that the analogy is not carried too far. For example, flow properties across a shock wave and hydraulic jump are not the same. Heil *et al.* report a Mach wave relationship over a range of supercritical flow velocities in their shallow free surface investigations while in a gas dynamics flow a Mach wave relationship holds only when the Mach number is equal to 1 (the shocks are infinitesimally weak and correspond to sound waves). A more complex, nonlinear relationship for the shock wave angle holds for Mach numbers greater than one.
[15] P. Heil, E. C. Rericha, D. I. Goldman, and H. L. Swinney, "Mach cone in a shallow granular fluid," Phys. Rev. E **70**, 060301 (2004).